nature medicine

Therapeutic cell engineering with surface-conjugated synthetic nanoparticles

Matthias T Stephan[1,2], James J Moon[1,2], Soong Ho Um[1–3], Anna Bershteyn[1,2] & Darrell J Irvine[1–5]

A major limitation of cell therapies is the rapid decline in viability and function of the transplanted cells. Here we describe a strategy to enhance cell therapy via the conjugation of adjuvant drug–loaded nanoparticles to the surfaces of therapeutic cells. With this method of providing sustained pseudoautocrine stimulation to donor cells, we elicited marked enhancements in tumor elimination in a model of adoptive T cell therapy for cancer. We also increased the *in vivo* repopulation rate of hematopoietic stem cell grafts with very low doses of adjuvant drugs that were ineffective when given systemically. This approach is a simple and generalizable strategy to augment cytoreagents while minimizing the systemic side effects of adjuvant drugs. In addition, these results suggest therapeutic cells are promising vectors for actively targeted drug delivery.

Cell-based therapies, such as hematopoietic stem cell (HSC), islet cell or hepatocyte transplants, are in routine clinical practice[1,2], and new treatment strategies implementing adult, embryonic or induced pluripotent stem cells are in various stages of development[3,4]. In the field of cancer immunotherapy, early clinical trials infusing *ex vivo*–expanded tumor-specific T lymphocytes have yielded promising results for the treatment of cancer and chronic infections[5–7]. Notably, after cell transfer, therapeutic cells often rely on the concurrent delivery of adjuvant drugs. These agents are designed to maximize donor cell efficacy and *in vivo* persistence, offset suppressive molecules at cell homing sites and promote the differentiation of transferred cells into a therapeutically optimal phenotype. Examples include γ_c receptor cytokines[5,8] or transforming growth factor-β signaling inhibitors[9] in adoptive T cell therapy or the use of small-molecule drugs to boost immune reconstitution after HSC transplants[10]. However, these agents often need to be maintained at high and sustained systemic levels for efficacy. This leads to dose-limiting toxicities for these drugs due to their generally pleiotropic activity, which has restricted their clinical use[11,12]. One approach to focus adjuvant drug action on the transferred cells is to genetically engineer donor cells to secrete their own supporting factors[13]. However, the regulatory and cost barriers of large-scale production and safety testing of clinical-grade vectors, costly and lengthy cell culture protocols and the technical challenges of efficient gene transfer hinder the implementation of clinical gene therapy protocols. Furthermore, several emerging adjuvant therapies are based on small-molecule drugs that cannot be genetically encoded[9,10]. Here we describe an alternate strategy for adjuvant drug delivery in cell therapies based on chemical conjugation of submicron-sized drug-loaded synthetic particles directly onto the plasma membrane of donor cells, enabling continuous pseudoautocrine stimulation of transferred cells *in vivo*.

RESULTS

Stable nanoparticle attachment to cell surfaces

To stably couple synthetic drug-carrier nanoparticles to the surface of therapeutic cells, we exploited the fact that many cells have high levels of reduced thiol groups on their surfaces[14]. Confirming previous reports[14], we detected substantial amounts of free thiols on the surfaces of T cells, B cells and HSCs but low amounts on red blood cells (**Fig. 1a**). To link synthetic drug carriers to cells via these surface thiols, we used liposomes and liposome-like synthetic nanoparticles 100–300 nm in diameter with a drug-loaded core and phospholipid surface layer, in which the lipid bilayer surface of the particles included thiol-reactive maleimide headgroups (**Supplementary Fig. 1**). We achieved particle conjugation by a simple two-step process (**Fig. 1b**): we first incubated donor cells with nanoparticles to permit maleimide-thiol coupling, followed by *in situ* conjugation to thiol-terminated polyethylene glycol (PEGylation) to quench residual reactive groups of the particles (**Supplementary Fig. 2**). With this approach, we could covalently link a substantial number of nanoparticles with diameters in the 100–300 nm range to cell types used commonly in cell therapy, including $CD8^+$ T lymphocytes or lineage$^-$Sca-1^+c-Kit^+ HSCs (**Fig. 1c**). Particles ranging from simple liposomes (with an aqueous drug-loaded core) to more complex multilamellar lipid nanoparticles or lipid-coated polymer nanoparticles[15] (**Fig. 1c** and **Supplementary Figs. 1** and **3**) were stably attached to live cells. Notably, particle coupling was benign, as coupling of up to 140 (± 30) ~200-nm multilamellar lipid nanoparticles to the surface of cells was nontoxic (**Supplementary Fig. 4**) and blocked only 17.2% (± 8.7%) of the total available cell surface thiol groups (**Supplementary Fig. 5**). These findings are consistent with a simple calculation of the surface area occupied by the nanoparticles:

[1]Department of Material Science and Engineering, Massachusetts Institute of Technology (MIT), Cambridge, Massachusetts, USA. [2]Koch Institute for Integrative Cancer Research, MIT, Cambridge, Massachusetts, USA. [3]Department of Biological Engineering, Massachusetts Institute of Technology, Cambridge, Massachusetts, USA. [4]Ragon Institute of Massachusetts General Hospital, MIT and Harvard University, Boston, Massachusetts, USA. [5]Howard Hughes Medical Institute, Chevy Chase, Maryland, USA. Correspondence should be addressed to D.J.I. (djirvine@mit.edu).

Received 7 January; accepted 5 May; published online 15 August 2010; doi:10.1038/nm.2198

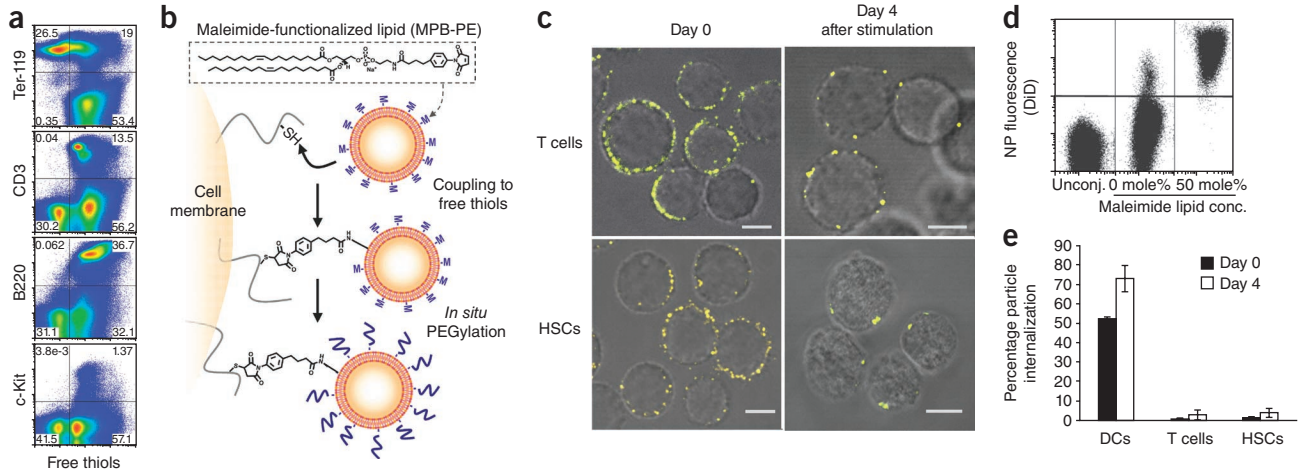

Figure 1 Stable conjugation of nanoparticles (NPs) to the surfaces of T cells and HSCs via cell-surface thiols. (**a**) Flow cytometry analysis of cell surface thiols on mouse splenocytes detected by fluorophore-conjugated malemide co-staining with lineage-specific surface markers for erythrocytes (Ter-119), T cells (CD3), B cells (B220) and hematopoietic stem cells (c-Kit). (**b**) Schematic of maleimide-based conjugation to cell surface thiols. MPB-PE, 1,2-dioleoyl-sn-glycero-3-phosphoethanolamine-*N*-[4-(p-maleimidophenyl)butyramide]. (**c**) Confocal microscopy images of $CD8^+$ effector T cells and lineage$^-$Sca-1^+c-Kit^+ HSCs immediately after conjugation with fluorescent 1,1-dioctadecyl-3,3,3,3-tetramethylindodicarbocyanine (DiD)-labeled multilamellar lipid nanoparticles (left) and after 4-d *in vitro* expansion (right). Scale bars, 2 μm. (**d**) Flow cytometry analysis of $CD8^+$ T cells after incubation with DiD-labeled multilamellar lipid nanoparticles synthesized with or without maleimide-headgroup lipids. (**e**) Quantification of nanoparticle internalization. Immature dendritic cells (DCs), effector $CD8^+$ T cells or HSCs were conjugated with carboxyfluorescein (CFSE)-tagged maleimide-bearing liposomes. Extracellular trypan blue quenching was used to differentiate surface-bound and internalized liposomes immediately after conjugation or after 4 d in culture. Data represent the mean ± s.e.m. of two independent experiments conducted in triplicate.

attachment of 150 particles, each 200 nm in diameter, would occlude only 3% of the surface of a typical 7-μm-diameter T cell.

Although liposomes and lipid-coated polymer particles spontaneously adsorbed to cell surfaces, we found that physically adsorbed particles could be removed during mild cell washing steps, whereas maleimide-linked particles remained stably bound to cells (**Fig. 1d**). Attachment of nanoparticles to T cells did not trigger spontaneous activation of the cells (**Supplementary Fig. 6**), and particles bound to lymphocytes or HSCs remained localized at the cell surface, as revealed by optical sectioning with confocal microscopy (**Fig. 1c** and **Supplementary Movies 1** and **2**) and by flow cytometry internalization assays (**Fig. 1e**), even after extended *in vitro* stimulation (**Fig. 1c**). In contrast, we observed that phagocytic cells such as immature dendritic cells efficiently internalized maleimide-functionalized nanoparticles after a short incubation (**Fig. 1e**). Although all three types of nanoparticles tested here conjugated to lymphocytes with comparable efficiencies, we chose to focus on ~300-nm multilamellar lipid nanoparticles (**Supplementary Fig. 1b**) for our subsequent *in vitro* functional and *in vivo* therapeutic studies on the basis of their high drug encapsulation efficiencies and week-long drug release profiles and the lack of inflammatory responses elicited from innate immune cells exposed to the 'empty' particles (**Supplementary Figs. 7** and **8**).

Nanoparticle conjugation does not alter key cellular functions

We next determined the maximum number of particles (without encapsulated drug cargo) that could be linked to cells without compromising key cellular functions, focusing on therapeutic cytotoxic T cells that must be capable of forming an immunological synapse and killing target cells, proliferating and secreting cytokines as part of their normal function. Ovalbumin-specific T cell receptor–transgenic OT-1 $CD8^+$ T cells conjugated with up to 100 (± 20) nanoparticles per cell retained an unmodified proliferative response after co-culture with ovalbumin-pulsed dendritic cells; higher surface densities of particles began to inhibit T cell proliferation (**Fig. 2a**, and **Supplementary Fig. 9a**,**b**). During cell division, surface-attached nanoparticles segregated equally to daughter cells, reflected by a stepwise decrease in

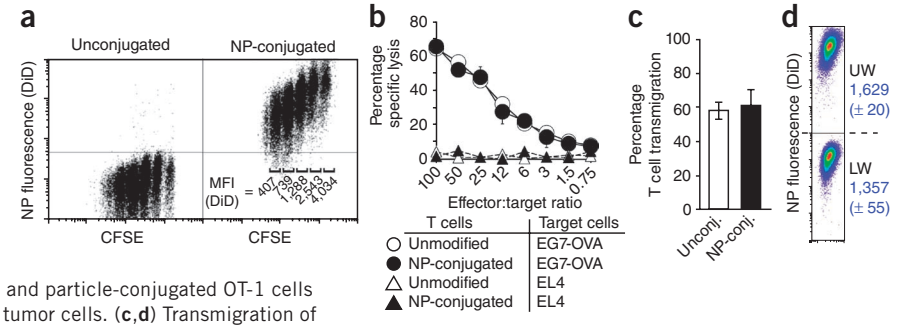

Figure 2 Nanoparticle conjugation does not affect key T cell functions. OT-1 ovalbumin-specific $CD8^+$ effector T cells were conjugated with 100 DiD-labeled multilamellar lipid nanoparticles per cell or left unmanipulated as controls. (**a**) CFSE dilution of unmodified or nanoparticle-conjugated T cells stimulated *in vitro* with mature ovalbumin peptide–pulsed dendritic cells. DiD mean fluorescence intensities (MFIs) for distinct CFSE lymphocytes populations are indicated in the bottom right quadrant. (**b**) ^{51}Cr release assays of unmanipulated and particle-conjugated OT-1 cells targeting ovalbumin peptide–pulsed or control EL4 tumor cells. (**c**,**d**) Transmigration of OT-1 T cells (with or without surface-bound particles) seeded onto MS1 endothelial cell monolayers in the upper well of a transwell chamber after addition of the chemoattractant monocyte chemoattractant protein-1 to the lower chamber. The fraction of transmigrating T cells (**c**) and the profile of cell-bound nanoparticle fluorescence before (UW) and after (LW) transmigration (**d**) were quantified by flow cytometry (DiD MFI ± s.e.m. from triplicate samples shown in blue).

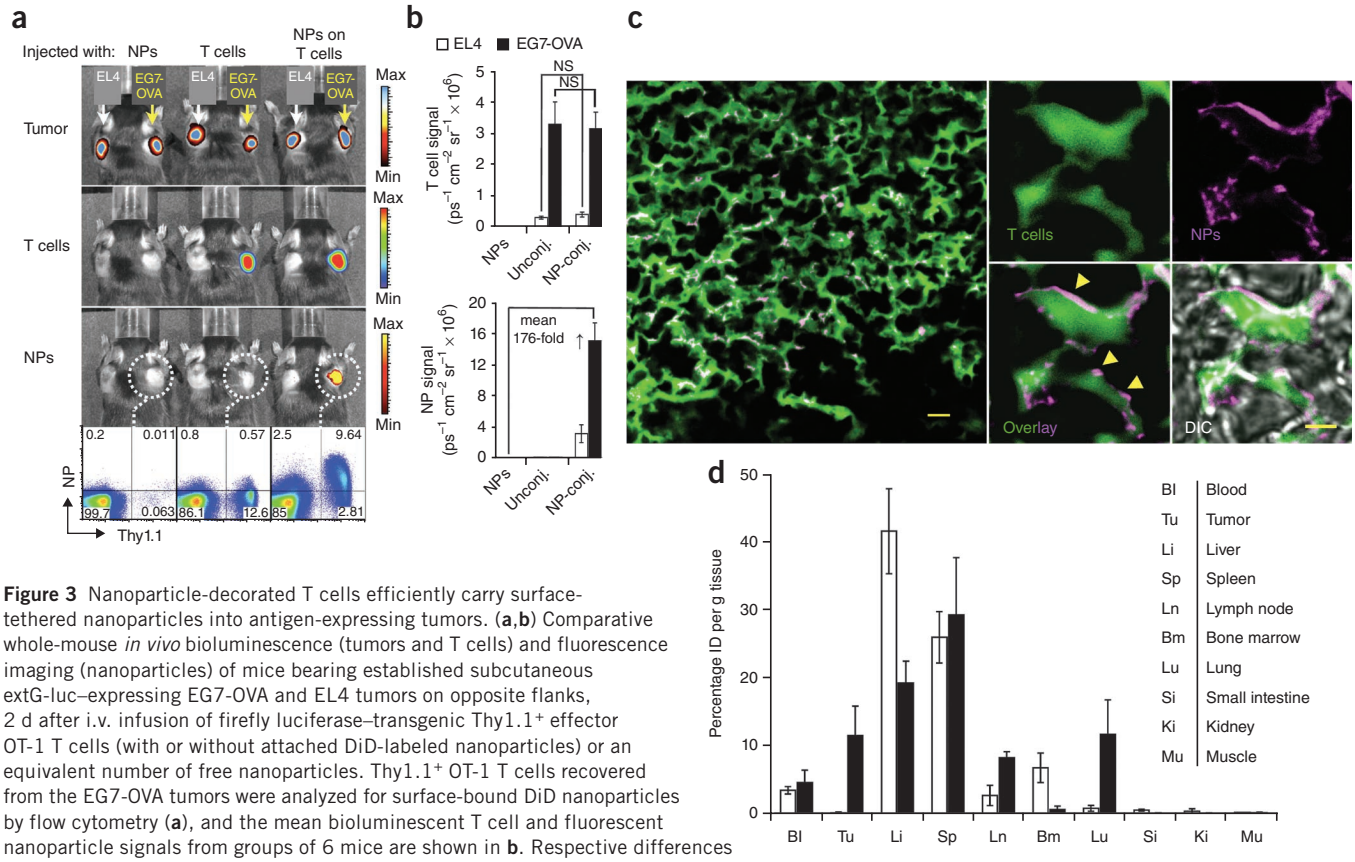

Figure 3 Nanoparticle-decorated T cells efficiently carry surface-tethered nanoparticles into antigen-expressing tumors. (**a**,**b**) Comparative whole-mouse *in vivo* bioluminescence (tumors and T cells) and fluorescence imaging (nanoparticles) of mice bearing established subcutaneous extG-luc–expressing EG7-OVA and EL4 tumors on opposite flanks, 2 d after i.v. infusion of firefly luciferase–transgenic Thy1.1$^+$ effector OT-1 T cells (with or without attached DiD-labeled nanoparticles) or an equivalent number of free nanoparticles. Thy1.1$^+$ OT-1 T cells recovered from the EG7-OVA tumors were analyzed for surface-bound DiD nanoparticles by flow cytometry (**a**), and the mean bioluminescent T cell and fluorescent nanoparticle signals from groups of 6 mice are shown in **b**. Respective differences in the bioluminescent or fluorescent photon counts of EL4 compared to EG7-OVA tumors were analyzed by the Student's *t* test. NS, not significant. ↑ refers to higher fluorescent signal strength of the data points on the right in comparison to respective values on the left. (**c**) Confocal images of nanoparticle-decorated OT-1 T cells infiltrating EG7-OVA tumor 2 d after adoptive transfer. Scale bar, 10 µm. Higher magnification images of nanoparticle-carrying tumor-infiltrating T cells are shown at right. Scale bars, 1.5 µm. Yellow arrowheads highlight evidence for surface localization of nanoparticles. Shown is one of two independent experiments. (**d**) Biodistribution of an equivalent number of DiD-labeled nanoparticles injected systemically (open bars) or conjugated to adoptively transferred OT-1 T cells (filled bars) after 48 h. The mean fluorescent signal intensities (± s.d.) of nine mice from three independent experiments are graphed. ID, injected dose. Data shown are pooled from three independent experiments.

the mean fluorescence emitted from cell-conjugated nanoparticles with increasing number of divisions (**Figs. 1c** and **2a**). Attachment of ~100 particles per cell also did not affect T cell recognition or killing of ovalbumin peptide–pulsed target cells or cytokine release profiles (**Fig. 2b** and **Supplementary Fig. 9c**). We next assessed the impact of cell surface–tethered nanoparticles on T cell transmigration across endothelial monolayers—a key capability of any therapeutic cell to efficiently infiltrate its target tissue. We first used an *in vitro* transwell co-culture system and quantified the migration of nanoparticle-conjugated T lymphocytes across a membrane-supported confluent endothelial monolayer in response to a chemoattractant placed in the lower chamber. T cells carrying 100 nanoparticles per cell showed unaltered transmigration efficiencies compared to unmodified cells (**Fig. 2c**). After crossing the endothelial barrier, T cells retained 83% (± 3%) of their original nanoparticle cargo physically attached (**Fig. 2d**). (In comparative experiments, liposomes and lipid-coated poly(lactic-co-glycolic acid) particles could also be carried through endothelial layers by T cells, although poly(lactic-co-glycolic acid) particles were not retained as well by transmigrating cells and showed a tendency to inhibit T cell transmigration at high particle-per-cell loadings; **Supplementary Fig. 10**).

To determine whether *in vivo* tissue homing of T cells was affected by nanoparticle conjugation, we evaluated the tumor-homing properties of particle-conjugated lymphocytes (**Fig. 3**). Subcutaneous EL4 tumors expressing membrane-bound *Gaussia* luciferase (extG-luc) and ovalbumin (EG7-OVA) or exG-luc alone were established on opposite flanks of C57BL/6 mice. Tumor-bearing mice then received adoptive transfers of firefly luciferase (F-luc)-transgenic OT-1 T cells with or without surface-conjugated red fluorescent nanoparticles or an intravenous (i.v.) injection of an equivalent dose of fluorescent particles alone. Particle-carrying OT-1 T cells specifically trafficked to EL4-OVA tumors (**Fig. 3a**), and we observed no difference in the tumor-homing potential of particle-conjugated compared to unmodified OT-1 T cells (**Fig. 3b**). Quantitative fluorescent particle imaging of EG7-OVA tumors indicated that nanoparticles accumulated 176-fold more efficiently at the tumor site when they were attached to the surface of OT-1 T cells compared to systemically infused free nanoparticles, which were rapidly scavenged by the liver and the spleen (**Fig. 3b**,**d**). Flow cytometry analysis independently verified that T cell infiltration of EG7-OVA tumors was quantitatively identical for particle-decorated and control OT-1 cells and that the majority of particle-conjugated cells recovered from tumors still retained their nanoparticle cargo (**Fig. 3a**). In separate experiments with fluorescently labeled OT-1 T cells, we confirmed prominent infiltration of nanoparticle-decorated T cells into EG7-OVA tumors in histological tumor sections examined by confocal microscopy, and

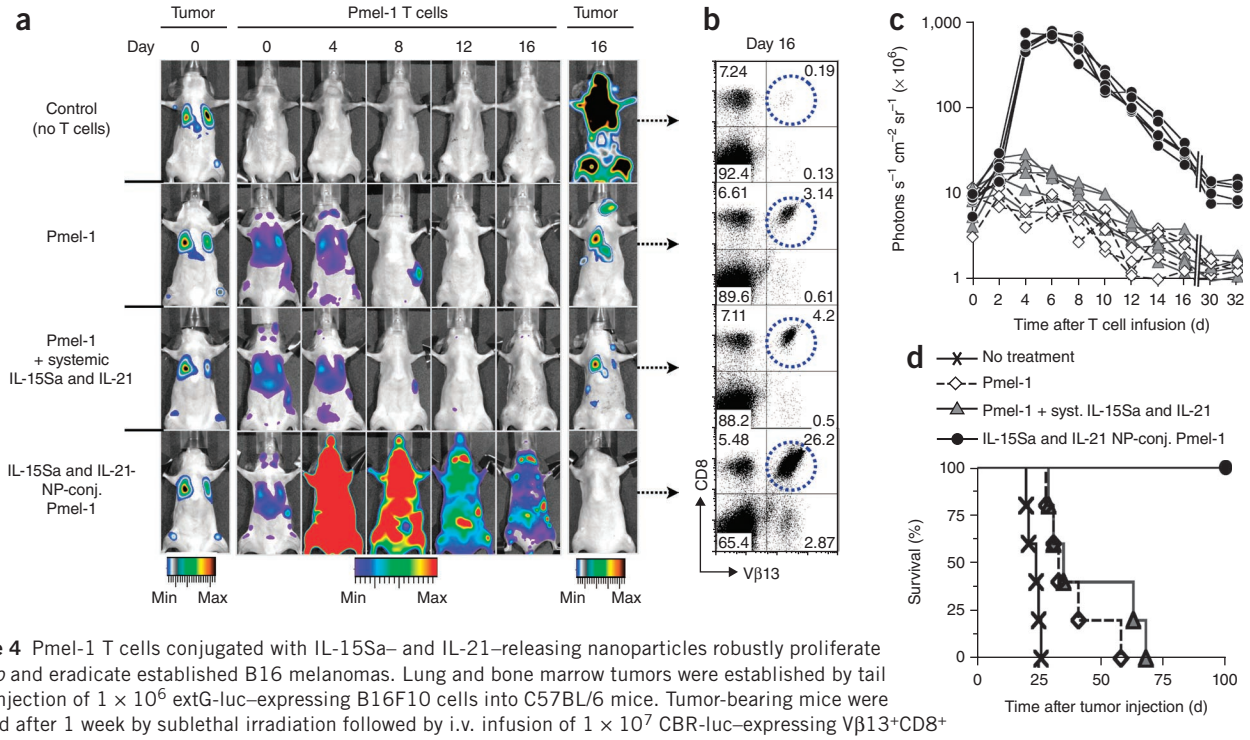

Figure 4 Pmel-1 T cells conjugated with IL-15Sa– and IL-21–releasing nanoparticles robustly proliferate *in vivo* and eradicate established B16 melanomas. Lung and bone marrow tumors were established by tail vein injection of 1×10^6 extG-luc–expressing B16F10 cells into C57BL/6 mice. Tumor-bearing mice were treated after 1 week by sublethal irradiation followed by i.v. infusion of 1×10^7 CBR-luc–expressing Vβ13$^+$CD8$^+$ Pmel-1 T cells. One group of mice received Pmel-1 T cells conjugated with 100 nanoparticles per cell carrying a total dose of 5 μg IL-15Sa and IL-21 (4.03 μg IL-15Sa + 0.93 μg IL-21); control groups received unmodified Pmel-1 T cells and a single systemic injection of the same doses of IL-15Sa and IL-21 or Pmel-1 T cells alone. (**a**) Dual longitudinal *in vivo* bioluminescence imaging of extG-luc–expressing B16F10 tumors and CBR-luc–expressing Pmel-1 T cells. (**b**) Frequencies of Vβ13$^+$CD8$^+$ Pmel-1 T cells recovered from pooled lymph nodes of representative mice 16 d after T cell transfer. (**c**) CBR-luc T cell signal intensities from sequential bioluminescence imaging every 2 d after T cell transfer. Every line represents one mouse, with each dot showing the whole-mouse photon count. (**d**) Survival of mice after T cell therapy illustrated by Kaplan-Meier curves. Shown are six mice per treatment group pooled from three independent experiments.

nanoparticles appeared to be localized to the surface, as observed *in vitro* (**Fig. 3c**, **Supplementary Fig. 11** and **Supplementary Movies 3** and **4**). Of note, the ability of lymphocytes to efficiently transfer surface-tethered nanoparticles across endothelial barriers *in vivo* was not restricted to the abnormal endothelial lining[16] found in tumor vasculature (**Supplementary Fig. 12**). When we linked particles to resting B cells expressing CC-motif chemokine receptor-7 and CD62 ligand (CD62L) (**Supplementary Fig. 12**) or central memory CD8$^+$ T cells (data not shown), particles were transported across the intercellular boundaries of high endothelial venules into lymph nodes—a poorly accessible compartment for systemically infused free nanoparticles.

Targeted cytokine support of antitumor T cells

We next tested whether cell-bound adjuvant drug–loaded nanoparticles could directly impart amplified therapeutic functions to their cellular carriers by treating established, disseminated B16F10 melanoma lung and bone marrow metastases with adoptively transferred melanoma-specific Pmel-1 CD8$^+$ T cells[17]. We encapsulated a mixture of the cytokines interleukin-15 (IL-15) (converted to a superagonist (IL-15Sa) by precomplexing with soluble IL-15 receptor α[18]) and IL-21 into multilamellar lipid nanoparticles. These two interleukins cooperatively promote *in vivo* T cell expansion and effector function when administered daily at high doses[8]. Particles ~300 nm in diameter efficiently entrapped IL-15Sa and IL-21 and released bioactive cytokine over a 7-d period (**Supplementary Fig. 13**). These cytokine-loaded particles were conjugated to CD8$^+$ Pmel-1 effector T cells expressing click beetle red (CBR)-luciferase (CBR-luc). Particle-conjugated or control T cells were infused into lymphodepleted mice bearing established *Gaussia* luciferase–expressing B16F10 melanoma lung and bone marrow tumors (**Fig. 4a**). Serial imaging of non-adjuvanted Pmel-1 T cells showed a gradual CBR-luc signal decline after T cell injection, consistent with poor *in vivo* T cell expansion and persistence (**Fig. 4a–c**). Whereas a single systemic infusion of 5 μg free cytokine (4.03 μg IL-15Sa plus 0.93 μg IL-21) given on the day of adoptive transfer did not significantly boost Pmel-1 proliferation (1.4-fold higher CBR-luc signal on day 6, $P = 0.32$), the same cytokine dose loaded in cell-bound nanoparticles elicited markedly amplified proliferation by Pmel-1 cells (81-fold higher peak photon count relative to unmodified Pmel-1 T cells on day 6, $P < 0.0001$, **Fig. 4a**,**c**). Subsequent to a contraction period, cytokine nanoparticle–carrying T cells showed enhanced long-term persistence (14.8-fold and 4.7-fold higher photon counts than Pmel-1 T cells alone at 16 and 30 d after T cell infusion, respectively, $P < 0.0001$) and homed as CD44$^+$CD62L$^+$ central memory T cells to lymph nodes and spleen (**Fig. 4a**,**b** and **Supplementary Fig. 14**).

Notably, experiments comparing the *in vivo* proliferative response of T cells bearing cytokine-loaded nanoparticles and bystander tumor-homing T cells showed that nanoparticle-released cytokines activated T cells primarily in *cis*, with limited paracrine stimulation of bystander cells (**Supplementary Fig. 15**). The adjuvant effect of T cell–conjugated cytokine nanoparticles was largely tumor antigen independent (**Supplementary Fig. 16b**,**d**), consistent with earlier studies demonstrating antigen-independent proliferation of T cells in response to IL-15 (ref. 19), but there was no evidence of progressive T cell clonality or leukemia formation in any treated mouse imaged at late time points (data not shown). Of note, cytokine-loaded

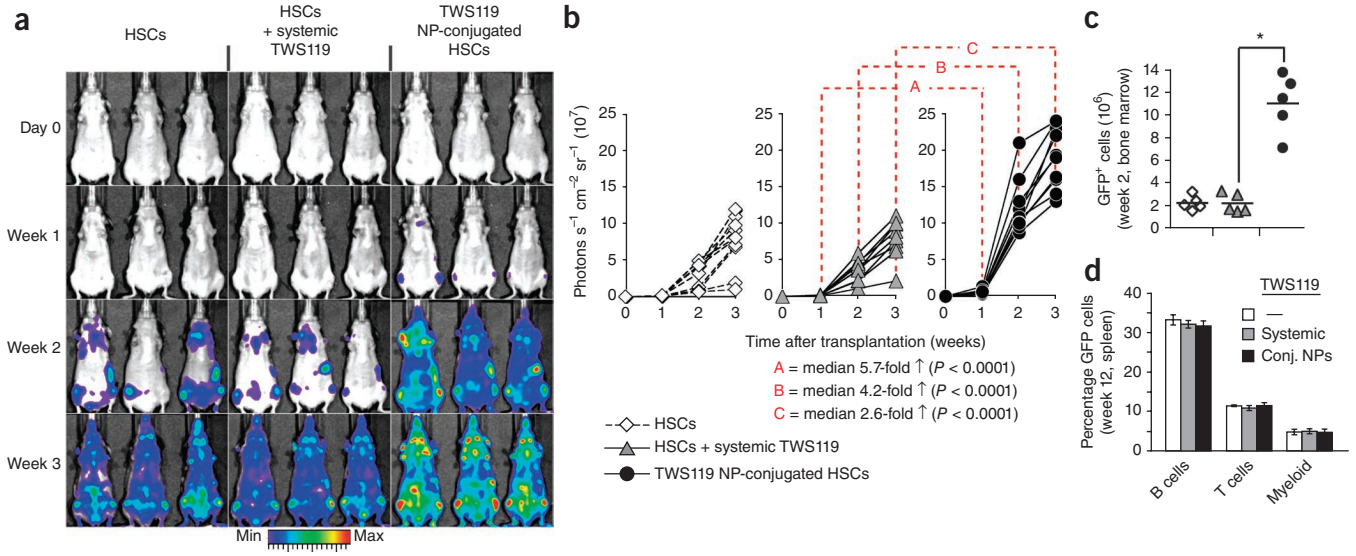

Figure 5 HSCs carrying GSK-3β inhibitor–loaded nanoparticles reconstitute recipient animals with rapid kinetics after bone marrow transplants without affecting multilineage differentiation potential. (**a**,**b**) Engraftment kinetics of luciferase-transgenic HSC grafts in lethally irradiated nontransgenic syngeneic recipients. Mice were treated with a single bolus injection of the GSK-3β inhibitor TWS119 (1.6 ng) on the day of transplantation, an equivalent TWS119 dose encapsulated in HSC-attached nanoparticles or no exogenous adjuvant compounds. Transplanted mice were imaged for whole-body bioluminescence every 7 d for 3 weeks. Shown are representative *in vivo* imaging system images (**a**) and whole-mouse photon counts (**b**) for nine mice total per treatment condition. (**c**) Percentage of donor-derived cells two weeks after transplantation of GFP$^+$ HSCs into lethally irradiated recipients with or without TWS119 adjuvant drug. *$P < 0.001$. (**d**) Average frequency of donor-derived GFP$^+$ B-cells, T cells and myeloid cells in five recipient mice per group (± s.d.) three months after transplantation are shown.

particles concurrently injected but not attached to T cells elicited a 4.9-fold higher peak Pmel-1 T cell proliferation compared to the same cytokine dose administered in an unencapsulated soluble form (day 6, $P = 0.0052$), but this stimulatory effect was still only 9% of that obtained by linking the same number of cytokine-loaded nanoparticles directly to the surface of the adoptively transferred T cells ($P < 0.0001$, **Supplementary Fig. 16c**,**d**). Pmel-1 T cells conjugated with empty nanoparticles showed the same expansion and decline *in vivo* as unmodified Pmel-1 cells (**Supplementary Fig. 16a**,**d**). All mice receiving cytokine nanoparticle–decorated Pmel-1 T cells achieved complete tumor clearance (**Fig. 4a**,**d**), whereas treatment with Pmel-1 T cells with or without systemic cytokine infusion at the same doses as encapsulated in nanoparticles yielded only modest survival advantages (**Fig. 4a**,**d**). We also investigated the *in vivo* tumor eradication potential of cytokine nanoparticle–conjugated Pmel-1 T lymphocytes in mice bearing large, established subcutaneous B16F10 flank tumors. Mice treated with unmodified Pmel-1 T lymphocytes uniformly succumbed to tumors within 30 d, whereas the infusion of cytokine nanoparticle–decorated Pmel-1 T cells prevented tumor growth, with all mice alive 30 d after T cell treatment (**Supplementary Fig. 17**).

Enhanced repopulation kinetics of HSC transplants

Prompted by the substantial therapeutic benefits achieved with conjugation of cytokine-loaded particles to tumor-specific T cells, we further examined the utility of this new adjuvant delivery approach in the context of hematopoietic stem cell transplantations. We chose the glycogen synthase kinase-3β (GSK-3β) inhibitor TWS119 (ref. 20) as therapeutic cargo on the basis of reports that repeated high-dose bolus therapy of transplant recipients with GSK-3 inhibitors enhances the repopulation kinetics of donor HSCs[10]. Multilamellar lipid nanoparticles efficiently encapsulated this small-molecule drug and slowly released it over a 7-d time period (**Supplementary Fig. 13**).

We evaluated the *in vivo* repopulation capabilities of hematopoietic grafts supported by cell-bound, TWS119-loaded nanoparticles on the basis of the whole-body photon emission from firefly luciferase–transgenic donor HSCs and, in separate experiments, by tracing the frequencies of GFP$^+$ donor HSCs by flow cytometry. After transplanting of lineage$^-$Sca-1$^+$c-Kit$^+$ HSCs from luciferase-transgenic donors into lethally irradiated syngeneic recipients, we observed a steady increase in whole-body bioluminescent emission originating from discrete foci over anatomic sites corresponding to the femurs, humeri, sternum and spleen (**Fig. 5a**). Whereas a systemic TWS119 bolus injection (1.6 ng) at the time of transplantation did not substantially alter measured engraftment kinetics (**Fig. 5a**,**b**), the same TWS119 dose encapsulated in nanoparticles surface tethered to donor HSCs significantly enhanced reconstitution by HSC grafts (median 5.7-fold higher bioluminescence than systemic TWS119 after 1 week, $P < 0.0001$, **Fig. 5a**–**c**). Notably, mice in all treatment groups initially engrafted HSCs in both femurs and the sternum, indicating that nanoparticle conjugation did not compromise the intrinsic homing properties of donor HSCs. Although conjugating TWS119 nanoparticles onto HSCs increased the rate of initial reconstitution, it did not affect their multilineage differentiation potential, reflected by a similar frequency of donor-derived GFP$^+$ reconstituted cell types compared to control HSC grafts 3 months after transplantation (**Fig. 5d**). Thus, this simple approach for donor cell modification just before cell transfer can also augment HSC transplants, a procedure in routine clinical practice.

DISCUSSION

Cell therapies (for example, HSC and islet cell transplants) are in common clinical practice and are also being aggressively developed in other areas of medicine, such as adoptive T cell therapy of cancer[5–7]. However, many cell therapy protocols rely on adjuvant

drugs that act directly on the transferred therapeutic cells to maintain their function, phenotype and/or lifespan. A ubiquitous challenge is the pleiotropic activity of many biological and small-molecule drugs, leading to toxicity or unwanted side effects after systemic exposure. This problem is illustrated by the use of IL-2 in the support of adoptive T cell therapy of melanoma, where IL-2 provides key adjuvant signals to donor T cells but also elicits severe dose-limiting toxicity[12].

Here we devised a simple, generalizable and clinically applicable strategy to augment the therapeutic potential of cytoreagents while limiting the potential for side effects from adjuvant drugs. We showed that adjuvant agent–releasing particles can be stably conjugated to cells without toxicity or interference with intrinsic cell functions, follow the characteristic *in vivo* migration patterns of their cellular vehicles and, ultimately, endow their carrier cells with substantially enhanced function using low drug doses that have no effect when given by traditional systemic routes. Prolonged retention of the particles on the surfaces of donor cells as shown here enables sustained drug release without concerns of premature degradation of the particle carrier or cargo owing to internalization into degradative intracellular compartments. Notably, previous work has shown that particles ~200 nm in diameter coated with antibody to CD3 are readily internalized by T cell lines[21], suggesting that internalization of particles in the size range studied here is not impossible for lymphocytes *per se*. Thus, elucidating the mechanisms regulating prolonged particle retention on T cell and HSC surfaces is an area for future study. Numerous reports have illustrated the potential of systemically infused nanoparticle materials slowly releasing drug cargos to enhance the efficacy of therapeutic drugs, and this has led to the development of clinical products such as anthracycline-loaded liposomes for cancer therapy[22]. However, in the context of support for cell therapy, our data demonstrate that conjugation of drug-loaded particles directly to the donor cells markedly increases their therapeutic impact. This strategy does not require cell preconditioning and complements traditional genetic engineering or chemical biology approaches[23] to augment or reprogram cell function. Given the wealth of available nanoparticle formulations tailored to deliver small molecule drugs, proteins, siRNA or magnetic imaging agents[24–27], the range of therapeutic or diagnostic cargos that can be attached to therapeutic cells probably extends far beyond the small molecules and recombinant proteins illustrated here.

Our study further demonstrates the concept of cells as chaperones that actively direct drug-loaded nanoparticles into poorly accessible anatomical compartments. In the field of cancer therapy, targeting strategies functionalizing drugs or biomaterials with specific tumor-targeting ligands, such as antibodies, aptamers, small molecules or folic acid, have been shown to improve therapeutic efficacy[28–30]. However, these approaches generally rely on the initially passive accumulation of targeted therapeutics at tumor sites via the enhanced permeation and retention effect[27], and it has been shown in some systems that targeting ligands do not change the overall tissue biodistribution of i.v.-delivered nanoparticle drug carriers but rather enable those particles that do reach tumors to be more efficiently internalized by target cells[28,31]. In contrast, cellular nanoparticle vectors actively transmigrate the endothelial barrier and accumulate cell-attached cargo in tissues at more than two-log greater levels than systemically infused free particles. This profoundly altered biodistribution opens new venues, beyond existing cell therapies, for applications of cell products as actively targeting drug delivery 'pharmacytes' or vaccine delivery tools.

METHODS

Methods and any associated references are available in the online version of the paper at http://www.nature.com/naturemedicine/.

Note: Supplementary information is available on the Nature Medicine website.

ACKNOWLEDGMENTS

This work was supported in part by the US National Institutes of Health (CA140476), the US National Science Foundation (Materials Research Science and Engineering Center award DMR-02-13282), Cancer Center Support (core) grant P30-CA14051 from the US National Cancer Institute and a gift to the Koch Institute by Curtis and Cathy Marble. D.J.I. is an investigator of the Howard Hughes Medical Institute. We thank M. Sadelain (Memorial Sloan-Kettering Cancer Center) for extG-luc and M. van den Brink (Memorial Sloan-Kettering Cancer Center) for F-luc–transgenic mice.

AUTHOR CONTRIBUTIONS

M.T.S. designed and conducted all experiments and wrote the manuscript. J.J.M. assisted in T cell transmigration assays, optimization of multilamellar lipid nanoparticle synthesis and *in vivo* nanoparticle biodistribution assays. S.H.U. assisted optimization of multilamellar lipid nanoparticle synthesis. A.B. assisted in initial *in vitro* T cell assays, collected electron microscopy images and contributed experimental suggestions. D.J.I. supervised all experiments and wrote the manuscript.

COMPETING FINANCIAL INTERESTS

The authors declare no competing financial interests.

Published online at http://www.nature.com/naturemedicine/.
Reprints and permissions information is available online at http://npg.nature.com/reprintsandpermissions/.

1. Fiorina, P., Shapiro, A.M., Ricordi, C. & Secchi, A. The clinical impact of islet transplantation. *Am. J. Transplant.* **8**, 1990–1997 (2008).
2. Alison, M.R., Islam, S. & Lim, S.M. Cell therapy for liver disease. *Curr. Opin. Mol. Ther.* **11**, 364–374 (2009).
3. Alper, J. Geron gets green light for human trial of ES cell–derived product. *Nat. Biotechnol.* **27**, 213–214 (2009).
4. Dimos, J.T. *et al.* Induced pluripotent stem cells generated from patients with ALS can be differentiated into motor neurons **321**, 1218–1221 (2008).
5. Morgan, R.A. *et al.* Cancer regression in patients after transfer of genetically engineered lymphocytes. *Science* **314**, 126–129 (2006).
6. Hunder, N.N. *et al.* Treatment of metastatic melanoma with autologous $CD4^+$ T cells against NY-ESO-1. *N. Engl. J. Med.* **358**, 2698–2703 (2008).
7. Mackinnon, S., Thomson, K., Verfuerth, S., Peggs, K. & Lowdell, M. Adoptive cellular therapy for cytomegalovirus infection following allogeneic stem cell transplantation using virus-specific T cells. *Blood Cells Mol. Dis.* **40**, 63–67 (2008).
8. Zeng, R. *et al.* Synergy of IL-21 and IL-15 in regulating $CD8^+$ T cell expansion and function. *J. Exp. Med.* **201**, 139–148 (2005).
9. Wallace, A. *et al.* Transforming growth factor-β receptor blockade augments the effectiveness of adoptive T cell therapy of established solid cancers. *Clin. Cancer Res.* **14**, 3966–3974 (2008).
10. Trowbridge, J.J., Xenocostas, A., Moon, R.T. & Bhatia, M. Glycogen synthase kinase-3 is an *in vivo* regulator of hematopoietic stem cell repopulation. *Nat. Med.* **12**, 89–98 (2006).
11. Berger, C. *et al.* Safety and immunological effects of IL-15 administration in nonhuman primates. *Blood* **114**, 2417–2426 (2009).
12. Thompson, J.A. *et al.* Recombinant interleukin 2 toxicity, pharmacokinetics and immunomodulatory effects in a phase I trial. *Cancer Res.* **47**, 4202–4207 (1987).
13. Treisman, J. *et al.* Interleukin-2–transduced lymphocytes grow in an autocrine fashion and remain responsive to antigen. *Blood* **85**, 139–145 (1995).
14. Sahaf, B., Heydari, K., Herzenberg, L.A. & Herzenberg, L.A. Lymphocyte surface thiol levels. *Proc. Natl. Acad. Sci. USA* **100**, 4001–4005 (2003).
15. Bernstein, I.D., Boyd, R.L. & van den Brink, M.R. Clinical strategies to enhance posttransplant immune reconstitution. *Biol. Blood Marrow Transplant.* **14**, 94–99 (2008).
16. Jain, R.K. A new target for tumor therapy. *N. Engl. J. Med.* **360**, 2669–2671 (2009).
17. Overwijk, W.W. *et al.* gp100/pmel 17 is a murine tumor rejection antigen: induction of 'self'-reactive, tumoricidal T cells using high-affinity, altered peptide ligand. *J. Exp. Med.* **188**, 277–286 (1998).
18. Rubinstein, M.P. *et al.* Converting IL-15 to a superagonist by binding to soluble IL-15Rα. *Proc. Natl. Acad. Sci. USA* **103**, 9166–9171 (2006).
19. Lu, J. *et al.* Interleukin 15 promotes antigen-independent *in vitro* expansion and long-term survival of antitumor cytotoxic T lymphocytes. *Clin. Cancer Res.* **8**, 3877–3884 (2002).

20. Gattinoni, L. *et al.* Wnt signaling arrests effector T cell differentiation and generates CD8+ memory stem cells. *Nat. Med.* **15**, 808–813 (2009).
21. Dinauer, N. *et al.* Selective targeting of antibody-conjugated nanoparticles to leukemic cells and primary T lymphocytes. *Biomaterials* **26**, 5898–5906 (2005).
22. Davis, M.E., Chen, Z.G. & Shin, D.M. Nanoparticle therapeutics: an emerging treatment modality for cancer. *Nat. Rev. Drug Discov.* **7**, 771–782 (2008).
23. Prescher, J.A., Dube, D.H. & Bertozzi, C.R. Chemical remodelling of cell surfaces in living animals. *Nature* **430**, 873–877 (2004).
24. Reddy, S.T. *et al.* Exploiting lymphatic transport and complement activation in nanoparticle vaccines. *Nat. Biotechnol.* **25**, 1159–1164 (2007).
25. Woodrow, K.A. *et al.* Intravaginal gene silencing using biodegradable polymer nanoparticles densely loaded with small-interfering RNA. *Nat. Mater.* **8**, 526–533 (2009).
26. Bin Na, H., Song, I.C. & Hyeon, T. Inorganic nanoparticles for MRI contrast agents. *Adv. Mater.* **21**, 2133–2148 (2009).
27. Tong, R. *et al.* Nanopolymeric therapeutics. *MRS Bull.* **34**, 422–431 (2009).
28. Bartlett, D.W., Su, H., Hildebrandt, I.J., Weber, W.A. & Davis, M.E. Impact of tumor-specific targeting on the biodistribution and efficacy of siRNA nanoparticles measured by multimodality *in vivo* imaging. *Proc. Natl. Acad. Sci. USA* **104**, 15549–15554 (2007).
29. Weissleder, R., Kelly, K., Sun, E.Y., Shtatland, T. & Josephson, L. Cell-specific targeting of nanoparticles by multivalent attachment of small molecules. *Nat. Biotechnol.* **23**, 1418–1423 (2005).
30. Dhar, S., Gu, F.X., Langer, R., Farokhzad, O.C. & Lippard, S.J. Targeted delivery of cisplatin to prostate cancer cells by aptamer functionalized Pt(IV) prodrug-PLGA-PEG nanoparticles. *Proc. Natl. Acad. Sci. USA* **105**, 17356–17361 (2008).
31. Kirpotin, D.B. *et al.* Antibody targeting of long-circulating lipidic nanoparticles does not increase tumor localization but does increase internalization in animal models. *Cancer Res.* **66**, 6732–6740 (2006).

ONLINE METHODS

Cell lines. The mouse melanoma cell line B16F10, the mouse pancreatic islet endothelial cell line MS1, the mouse thymoma cell line EL4 and EG7-OVA, an EL4 cell line stably transfected with the plasmid pAc-neo-OVA which carries a complete copy of chicken ovalbumin (OVA) mRNA, were all purchased from the American Type Culture Collection. We purchased the Phoenix Eco retroviral packaging cell line from Orbigen. For bioluminescent *in vivo* tumor imaging, we retrovirally transduced the B16F10, EL4 and EG7-OVA cell lines with a membrane-anchored form of the *Gaussia* luciferase (extG-Luc), provided to us by M. Sadelain, as described in the **Supplementary Methods**.

Mice and *in vivo* tumor models. Mice were housed in the MIT Animal Facility. We performed all mouse studies in the context of an animal protocol approved by the MIT Division of Comparative Medicine following federal, state and local guidelines. C57BL/6 mice, C57BL/6 Pmel-1–Thy1.1 mice, OT-1 transgenic mice and C57BL/6 GFP-transgenic mice were all obtained from Jackson Laboratories. C57BL/6 (H-2K^b, Thy-1.1) firefly luciferase (F-luc)-transgenic mice[32] were provided to us by M. van den Brink. For adoptive T cell experiments with ovalbumin-specific transgenic T cells, we subcutaneously injected C57BL/6 mice with 4×10^6 EG7-OVA tumor cells into the right flank and 2×10^6 control EL4 cells into the left flank to generate equally sized s.c. tumors 7 d later. We retrovirally transduced both tumor cell lines with extG-luc for bioluminescent imaging. To establish melanoma lung tumor metastases, we injected 1×10^6 B16F10-extG-luc tumor cells i.v. via the tail vein into C57BL/6 mice 1 week before T cell treatment. On the day of adoptive Pmel-1 T cell transfer, we sublethally irradiated recipient mice with 500 cGy of total body irradiation from a ^{137}Cs source. All mice were treated with a single infusion of 1.5×10^7 effector CD8$^+$ T cells.

Preparation of primed T cells for adoptive transfer and retroviral transduction. Spleens were collected, macerated over a filter, and resuspended in ACK lysing Buffer (Biosource). In all, we placed 3×10^6 splenocytes per milliliter in complete RPMI 1640 with 1 ng ml^{-1} IL-7 and 2 μg ml^{-1} concavalin A (Calbiochem) and incubated at 37 °C. Two days later, we removed dead cells by Ficoll gradient (GE Healthcare) and isolated CD8$^+$ cells with a mouse CD8 Negative Isolation Kit (Stemcell Technologies). We then preloaded 1 ml per well of concentrated retrovirus (**Supplementary Methods**) on six-well non–tissue-culture–treated dishes coated with RetroNectin (TakiraBio) and incubated them at 37 °C incubation for 1 h. An equal volume of isolated T cells (3×10^6 cells per ml substituted with 50 international units human IL-2 per ml) was added and centrifuged at 2,000*g* for 30 min. Six hours after 'spinoculation', 1 ml of fresh, prewarmed RPMI, containing 50 international units human IL-2 (Chiron) was added. We used T cells for adoptive transfer experiments 1 d after gene transfer.

Nanoparticle conjugation with cells and *in situ* PEGylation. Detailed information on nanoparticle and liposome synthesis as well as cytokine and small-molecule particle loading is included in the **Supplementary Methods**. We resuspended 6×10^7 cells per ml in serum-free X-Vivo 10 medium (Cambrex) after two PBS washes. We then added an equal volume of nanoparticles in nuclease-free water, with 1, 200, 600, 300 or 150 nanoparticles per T cell (resulting in 139 ± 29, 128 ± 23, 100 ± 21 or 75 ± 32 surface-tethered particles per T cell, respectively, after cell washes and PEGylation), and incubated the cells at 37 °C for 30 min with gentle agitation every 10 min. After a PBS wash to separate cells from unbound particles, we quenched residual maleimide groups on cell-bound particles by incubation of 3×10^6 cells per ml with 1 mg ml^{-1} thiol-terminated 2-kDa PEG (Laysan Bio) at 37 °C for 30 min in complete RPMI medium, followed by two PBS washes to remove unbound PEG.

We found 1 mg ml^{-1} thiol-PEG to be the optimal concentration required to quench all remaining maleimide groups on nanoparticles after cell conjugation on the basis of little FACS signal after a 30-min incubation with 70 mg ml^{-1} BODIPY-tagged cysteine (generated from reduction of the disulfide bond in BODIPY L-cystine (Invitrogen) with a 15-molar excess of HCl Tris(2-carboxyethyl) phosphine hydrochloride (Thermo Scientific) for 45 min at 37 °C). The nanoparticle binding efficiency of maleimide-functionalized (50 mol% 1,2-dioleoyl-sn-glycero-3-phosphoethanolamine-*N*-[4-(p-maleimidophenyl) butyramide] in the lipid fraction) multilamellar lipid nanoparticles to effector T lymphocytes was 33.4% (± 6.9%), when incubating 500 particles per T cell, as determined by high-magnification confocal microscopy imaging of 30 single T cell Z-stacks. We distinguished between surface-conjugated and internalized nanoparticles by flow cytometry internalization assay, described in the **Supplementary Methods**.

Statistical analyses. We used the unpaired Student's *t* test to test the difference between bioluminescent signals and the log-rank test to analyze survival data. All statistical analysis was performed using Prism 4.0 software.

Functional *in vitro* T cell and hematopoietic stem cell assays, hematopoietic stem cell transplantation, *in vivo* bioluminescence and fluorescence imaging, nanoparticle biodistribution assay, flow cytometry and confocal microscopy. Detailed information on *in vitro* T cell and HSC assay, transplantation, serial bioluminescent imaging and confocal microscopy assays are included in the **Supplementary Methods**.

32. Reichardt, W. *et al.* Impact of mammalian target of rapamycin inhibition on lymphoid homing and tolerogenic function of nanoparticle-labeled dendritic cells following allogeneic hematopoietic cell transplantation. *J. Immunol.* **181**, 4770–4779 (2008).

doi:10.1038/nm.2198